JBC RESEARCH ARTICLE

# The unique Phe–His dyad of 2-ketopropyl coenzyme M oxidoreductase/carboxylase selectively promotes carboxylation and S–C bond cleavage

Received for publication, April 27, 2021, and in revised form, June 29, 2021 Published, Papers in Press, July 12, 2021,
https://doi.org/10.1016/j.jbc.2021.100961

**Gregory A. Prussia[1], Krista A. Shisler[1], Oleg A. Zadvornyy[1], Bennett R. Streit[2], Jennifer L. DuBois[2], and John W. Peters[1,*]**

*From the [1]Institute of Biological Chemistry, Washington State University, Pullman, Washington, USA; [2]Department of Chemistry and Biochemistry, Montana State University, Bozeman, Montana, USA*

Edited by Ruma Banerjee

**The 2-ketopropyl-coenzyme M oxidoreductase/carboxylase (2-KPCC) enzyme is the only member of the disulfide oxidoreductase (DSOR) family of enzymes, which are important for reductively cleaving S–S bonds, to have carboxylation activity. 2-KPCC catalyzes the conversion of 2-ketopropyl-coenzyme M to acetoacetate, which is used as a carbon source, in a controlled reaction to exclude protons. A conserved His–Glu motif present in DSORs is key in the protonation step; however, in 2-KPCC, the dyad is substituted by Phe–His. Here, we propose that this difference is important for coupling carboxylation with C–S bond cleavage. We substituted the Phe–His dyad in 2-KPCC to be more DSOR like, replacing the phenylalanine with histidine (F501H) and the histidine with glutamate (H506E), and solved crystal structures of F501H and the double variant F501H_H506E. We found that F501 protects the enolacetone intermediate from protons and that the F501H variant strongly promotes protonation. We also provided evidence for the involvement of the H506 residue in stabilizing the developing charge during the formation of acetoacetate, which acts as a product inhibitor in the WT but not the H506E variant enzymes. Finally, we determined that the F501H substitution promotes a DSOR-like charge transfer interaction with flavin adenine dinucleotide, eliminating the need for cysteine as an internal base. Taken together, these results indicate that the 2-KPCC dyad is responsible for selectively promoting carboxylation and inhibiting protonation in the formation of acetoacetate.**

Biological $CO_2$ fixation reactions are essential drivers of the global carbon cycle, drawing atmospheric carbon into biomass and thereby helping to modulate the global thermostat. $CO_2$-fixing carboxylases are biochemically diverse and taxonomically widespread (1).

2-Ketopropyl-coenzyme M oxidoreductase/carboxylase (2-KPCC) is a member of the well-characterized NAD(P)H/flavin adenine dinucleotide (FAD)–dependent disulfide oxidoreductase (DSOR) family and a highly unusual bacterial carboxylase (2, 3). DSOR enzymes contain a redox-active cysteine pair that catalyzes the two-electron and two-proton reduction of a disulfide substrate (4–6), where GSSG reduction, catalyzed by glutathione reductase (GR), is a paradigmatic example (Fig. 1*B*) (7–10). An FAD cofactor relays the two electrons and one proton (net hydride, H–) from NADPH to the disulfide and then interacts electrostatically with the reduced Cys dithiol to maintain its reactive protonation state. The second proton needed for the reaction is relayed from a conserved active site histidine (11, 12). By contrast, 2-KPCC reductively cleaves the thioether bond of its 2-ketopropyl-CoM (2-KPC) substrate to yield an unstable enolacetone intermediate. This then attacks $CO_2$ to generate the acetoacetate product anion and CoM (Figs. 1*C* and 2) (13–15). In this way, 2-KPCC uniquely repurposes the DSOR scaffold to achieve carboxylase chemistry.

Catalytic efficiency in DSORs is reported to depend on a His–Glu pair known as the "catalytic dyad" (16). The conserved His shuttles protons to the substrates and stabilizes a charge transfer (CT) interaction between the FAD and one of the catalytic cysteines ($Cys_{CT}$) when the DSOR is in its reduced and reactive form. The Glu hydrogen bonds to the conserved His through its imidazole δ-N, orienting the side chain and lowering its $pK_a$ (11, 12). In 2-KPCC, the His–Glu dyad is substituted by a phenylalanine and histidine (F501 and H506, respectively). We hypothesize that these amino acid substitutions are essential for making 2-KPCC an effective carboxylase. Prior work with the 2-KPCC F501H variant indeed showed that F501 serves an essential role in restricting protonation of the enolacetone intermediate (Fig. 1*A*, step *[3]*), as this substitution resulted in near-complete conversion of 2-KPC to the unproductive protonation product acetone (2).

Carboxylases operate *via* a shared mechanistic logic that defines canonical behavior (Fig. 1*A*). A nucleophilic substrate or an anionic substrate, often in the form of an enolate, is stabilized by the enzyme and serves as a nucleophile toward $CO_2$ (17). The $CO_2$ is either entrapped inside the protein as a molecule of solubilized gas or released on demand—from carboxybiotin or carboxyphosphate, for example—adjacent to the enolate. The sp-hybridized carbon of $CO_2$ is bent and

* For correspondence: John W. Peters, jw.peters@wsu.edu.

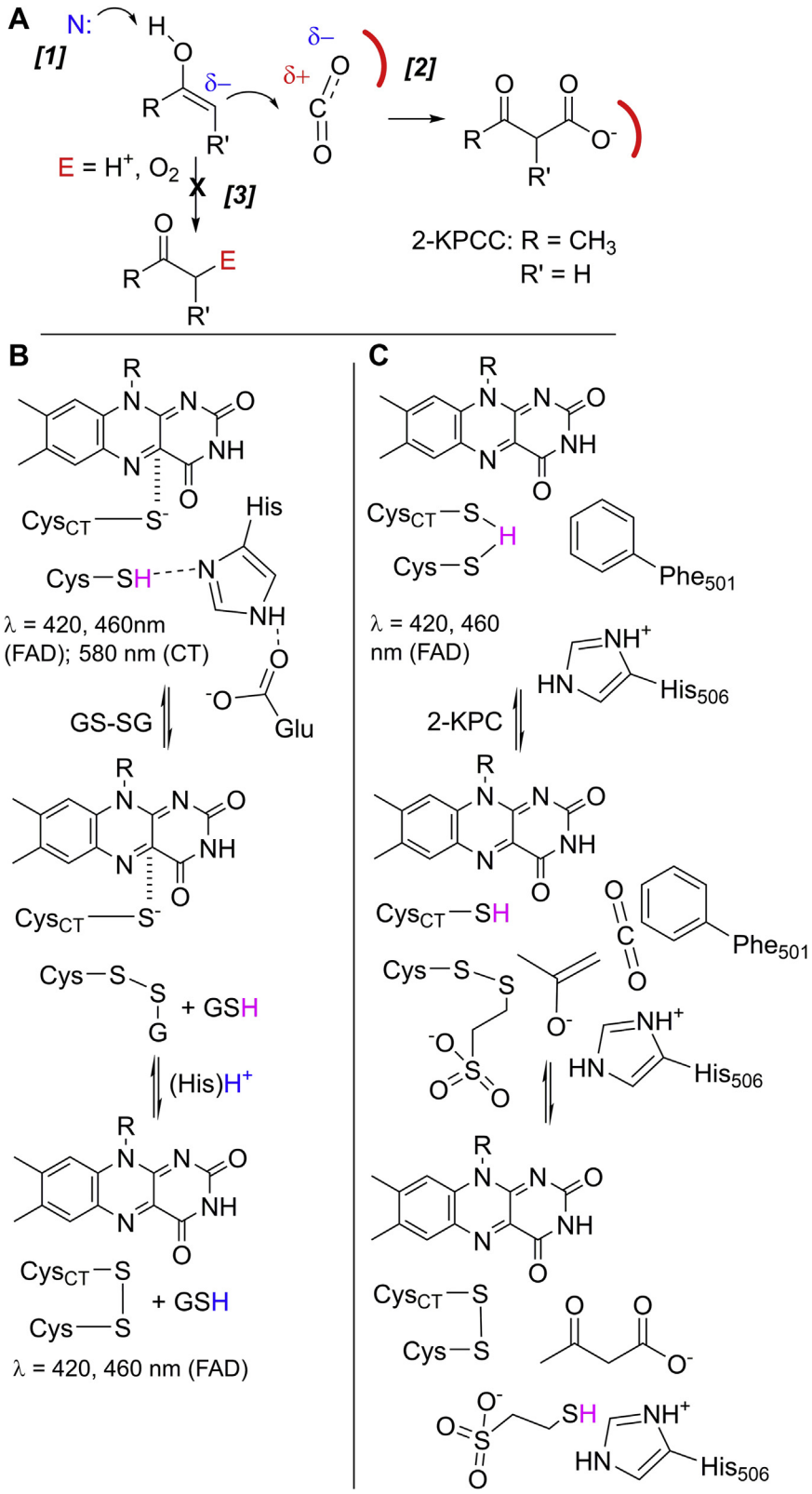


**Figure 1. Understanding how a DSOR catalyzes a carboxylation reaction.** *A*, general reaction catalyzed by carboxylases and resulting carboxylate product. E represents an electrophile, and the *red semicircle* an electropositive zone in the enzyme. [1] The substrate is first activated by the enzyme to yield an unstable and deprotonated ketone/enolate nucleophile. [2] The ketone/enolate can then attack $CO_2$ (shown distorted toward $sp^2$ hybridization) to produce the carboxylation product, such as acetoacetate in 2-KPCC. [3] In an undesired side reaction, the ketone/enolate can attack $H^+$ or $O_2$, producing the protonated product, such as acetone in 2-KPCC. *B*, reaction catalyzed by a representative DSOR, glutathione reductase (GR). The first structure depicts the active site in its NADPH-reduced catalytically active form. The *hashed line* indicates a charge transfer (CT) interaction between the active-site $Cys_{CT}$ (87) and the oxidized FAD, giving rise to UV–visible features with the listed maxima. The His–Glu catalytic dyad, which acts as a proton shuttle, and the two protons required for the reaction, are highlighted in *color*. *C*, reaction catalyzed by 2-KPCC. The first structure illustrates its reduced, reactive form, which contains a

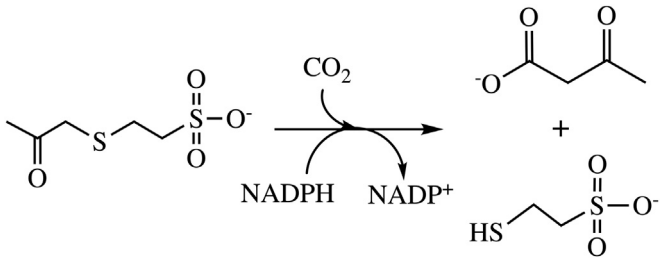


**Figure 2. Carboxylation of 2-KPC by 2-KPCC to produce acetoacetate and coenzyme M (CoM).** During turnover, NADPH is oxidized to NADP+. 2-KPC, 2-ketopropyl-CoM; 2-KPCC, 2-ketopropyl-coenzyme M oxidoreductase/carboxylase.

polarized in the transition state that forms en route to the product carboxylate. Finally, an efficient carboxylase protects the reactive enolate from electrophiles that could potentially compete with $CO_2$ (18). For example, Rubisco, earth's most abundant carboxylase (19), shields its reactive enolate from $O_2$, a much more abundant electrophile; the fact that it does so imperfectly leads to Rubisco's observed oxygenated side products.

Here, the F501H and H506E single and F501H_H506E double variants, in which one or both residues of the 2-KPCC catalytic dyad are exchanged for the characteristic His–Glu pair of a typical DSOR, were used to test the hypothesis that F501 and H506 are responsible for endowing a typical DSOR with the essential attributes of a carboxylase. In conjunction with X-ray structural, spectroscopic, and catalytic data, we provide evidence that the noncanonical F501–H506 dyad of 2-KPCC promotes the canonical steps of carboxylation chemistry in Figure 1*A* by stabilizing the carboxylic acid product as well as the reactive protonation state of the active site.

## Results and discussion

Members of the DSOR family of enzymes are best known for their roles in sulfur metabolism, where they reductively cleave disulfide bonds. We hypothesized that, despite being a member of the DSOR family, 2-KPCC would maintain much of the same chemical logic as other carboxylases in its catalytic conversion of 2-KPC and $CO_2$ to CoM and acetoacetate (Fig. 2). We further hypothesized that carboxylase chemistry would be encoded in the unique F501–H506 catalytic dyad of 2-KPCC, which replaces the canonical His–Glu of DSORs. These hypotheses were tested here using 2-KPCC with one or both residues of its dyad substituted by DSOR residues, with key results as follows:

### *F501 is optimally situated to block proton access to the reactive enolate intermediate*

We began by testing the hypothesis that the phenylalanine in the dyad (F501) of 2-KPCC is chiefly responsible for excluding electrophilic protons from the 2-KPCC active site (Fig. 1*A*, step *[3]*). We previously showed that protonation of the enolacetone intermediate, resulting in toxic acetone, was strongly favored by the F501H substitution (2). The product ratio shifted from 0% acetone (WT 2-KPCC) to 90% acetone (F501H; Table 1). Notably, the overall rate of NADPH turnover remained relatively unchanged in the F501H variant relative to WT. Moreover, acetone formation by F501H was comparable in rate to the carboxylation reaction catalyzed by WT 2-KPCC and leading to acetoacetate. These results are consistent with kinetic analyses that showed that Cys–disulfide reduction by NADPH is rate limiting in 2-KPCC (3) and insensitive to the F501H substitution.

To provide further insight into the validity of this interpretation, we determined the structure of the F501H variant and refined it to a resolution of 1.85 Å. The differences in the structure were restricted to the active-site region in proximity to the substitution. Crystals were grown in the presence of the substrate 2-KPC and, as in previous structures (14, 15, 20), was captured in the Cys–S–S–CoM disulfide state, which resulted from the reaction with 2-KPC during crystallization (Fig. 3). Moreover, His at the 501 position overlaps perfectly with the cognate dyad residue of GR, H467 (Fig. 3). This side chain occupies a central position between the Cys pair and the Cys-product mixed disulfide, where it has been shown to act as an essential active site acid–base (12). These structures strongly support the conclusion that the F501H variants, like WT GR, have an optimally positioned His that acts as a source of water-derived protons during turnover. This pathway for proton entry is effectively eliminated by the F501 side chain in WT 2-KPCC, which protects the enolacetone intermediate from water and/or side-chain bound $H^+$ that could compete with $CO_2$ as an electrophile (Fig. 1*A*). This model supports the hypothesis that we put forth nearly 20 years ago to explain the differences observed in the catalytic dyad residues of 2-KPCC relative to GR.

Our recent work has suggested that the catalytic dyad differences observed in 2-KPCC go beyond that of simply limiting protonation in the promotion of carboxylation. We have shown that 2-KPCC operates through a different key reactive intermediate than GR (3) in which the reduced state of the redox active dithiol exists with a bridged single proton instead of the FAD–$Cys_{CT}$ species observed in GR (Fig. 1, *B* and *C*). We can see in our structure of the F501H variant and the structure of GR that the interactions of His with the exchange thiol ($Cys_{INT}$ (C82)) would promote the stabilization of the GR-type reduced reactive intermediate relative to the 2-KPCC intermediate through stabilizing the more formal thiolate. We have attributed these differences in reactive intermediates observed between 2-KPCC and GR as yet another mechanism to limit proton access and promoting carboxylation. This is very much in line with the results of the reactivity of the F501H variant having substantial reductive thioether bond cleavage but markedly suppressed carboxylation activity (Table 1).

single proton shared between the two cysteines and no CT species or resulting band in the UV–visible spectrum. The Phe–His catalytic dyad that distinguishes 2-KPCC from canonical DSORs is shown. The reactive proton, which is shared between the catalytic cysteines and is transferred to CoM, is highlighted in *color*. 2-KPCC, 2-ketopropyl-coenzyme M oxidoreductase/carboxylase; CoM, coenzyme M; DSOR, disulfide oxidoreductase; FAD, flavin adenine dinucleotide.

**Table 1**
**Specific activities and product analyses for WT 2-KPCC and dyad variants support key roles for each in specifying carboxylation reactivity**

| 2-KPCC Enzyme | NADPH oxidation (nmol $min^{-1}$ $mg^{-1}$)[a] | Acetoacetate production (nmol $min^{-1}$ $mg^{-1}$)[b] | Acetone production (nmol $min^{-1}$ $mg^{-1}$) | Acetoacetate (%) |
|---|---|---|---|---|
| WT | 517.0 (8.8) | 284.5 (62)[c] | ND | 100 |
| F501H | 452.7 (10.6) | 22.1 (0.70)[c] | 224 (51)[c] | 10 |
| H506E | 326.0 (3.3) | 16.2 (3.3) | 27.1 (3.2) | 37 |
| F501H_H506E | 189.7 (2.8) | ND | 61.6 (7.1)[c] | 0 |

Abbreviation: ND, no detectable activity.
[a] Oxidation of NADPH was monitored as a decrease in UV–visible absorbance at 340 nm *via* 2-KPCC–dependent 2-KPC oxidation of NADPH (60 mM $KHCO_3$, 5 mM 2-KPC, and 0.25 mg 2-KPCC).
[b] Carboxylation of 2-KPC was monitored *via* the rate of decrease in UV–visible absorbance at 340 nm as described by the coupled assay (2, 21).
[c] Rates from Ref. (2).

### *H506 defines a likely site for $CO_2$ binding and conversion to the carboxylate moiety of the acetoacetate product*

$CO_2$ binding, deviation toward $sp^2$ hybridization, and development of negative charge in the ultimate carboxylation product (acetoacetate) are expected to be promoted by electropositive side chains in the active-site pocket (Fig. 1) (14, 20). In previous structures, we observed the binding of molecules assigned as anionic ligands derived from the crystallization solution in a small pocket that is flanked by Arg365 and His506, where His506 is at the analogous position of the Glu residue at the second position of the GR catalytic His–Glu dyad. We hypothesized, in line with the functional differences associated with the first residue of the dyad (Phe in 2-KPCC at the position of His in GR) that the second difference (His in 2-KPCC relative to Glu in GR) is also mechanistically relevant in having a role in promoting the unique carboxylation activity of 2-KPCC. Specifically, the anion-binding pocket may stabilize the developing charge incurred during carboxylation, thereby facilitating carboxylation and acetoacetate formation.

To address this potential role, we determined the structure of the F501H_H506E variant and refined it to a resolution of 1.8 Å (Fig. 4). In comparing the structure of the variant and WT 2-KPCC with that of GR, we observe that the analogous residue in the GR dyad, E472, is not in the same position as 506 in 2-KPCC, as shown in WT 2-KPCC in Figure 3. In GR, the E472 carboxylate side chain is positioned within hydrogen bonding distance to H468 and acts to modulate its $pK_a$. The different position of E506 in 2-KPCC is a likely result of differences in the isomeric state of the Pro in 2-KPCC (*trans*) *versus* GR (*cis*). In addition, the position of the Pro in the short region between the catalytic dyad residues in 2-KPCC ($F_{501}LNPTH_{506}$) *versus* GR ($H_{467}PTSSE_{472}$) results in differences in the backbone conformation. These differences presumably are important for the formation of an anion-binding pocket at this position in 2-KPCC. The unique position, dramatic difference in electrostatic character, and open cavity supported by the H506 residue in WT 2-KPCC all point toward a possible role in promoting carboxylation through a site that would stabilize the developing charge incurred during the formation of the product acetoacetate.

We further examined the hypothesis that the 2-KPCC H506 residue is involved in stabilizing the developing charge in the formation of the anionic acetoacetate product in two ways, focusing on the H506E and F501H single and the F501H_H506E double variants. First, we considered the impact of the H506E substitution on the product outcome. The H506E variant exhibited a dramatic shift toward acetone as the primary reaction product (63%; Table 1). If H506 is the site of $CO_2$ binding, polarization, and acetoacetate formation, the H506E substitution could favor acetone production by electrostatically blocking $CO_2$ binding and/or acetoacetate formation (Fig. 1*A*, step *[2]*). In the absence of a carboxylation reaction, the enolacetone intermediate is expected to linger until water-mediated protonation could occur. In fact, acetone was produced at an approximately 10-fold slower rate in 2-

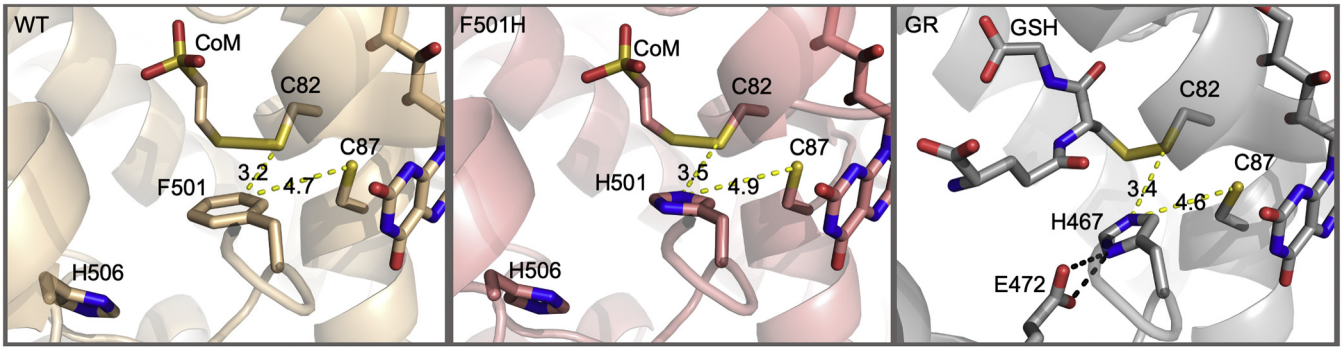


**Figure 3. The His (or Phe) half of the dyads in 2-KPCC, F501H active-site variant, and GR occupy similar positions relative to the active-site cysteines in the mixed disulfide state.** The dyad of WT 2-KPCC (*left*), F501H (*middle*), and GR (*right*) is shown with distances between the Phe (2-KPCC) or His (2-KPCC F501H variant and GR) to the catalytic cysteines. In each case, $Cys_{INT}$ (C82) is shown making a mixed disulfide with the substrate. Protein Data Bank file of WT 2-KPCC: 2C3C; F501H variant: 7MGO; and GR: 1GRE. 2-KPCC, 2-ketopropyl coenzyme M oxidoreductase/carboxylase; GR, glutathione reductase.

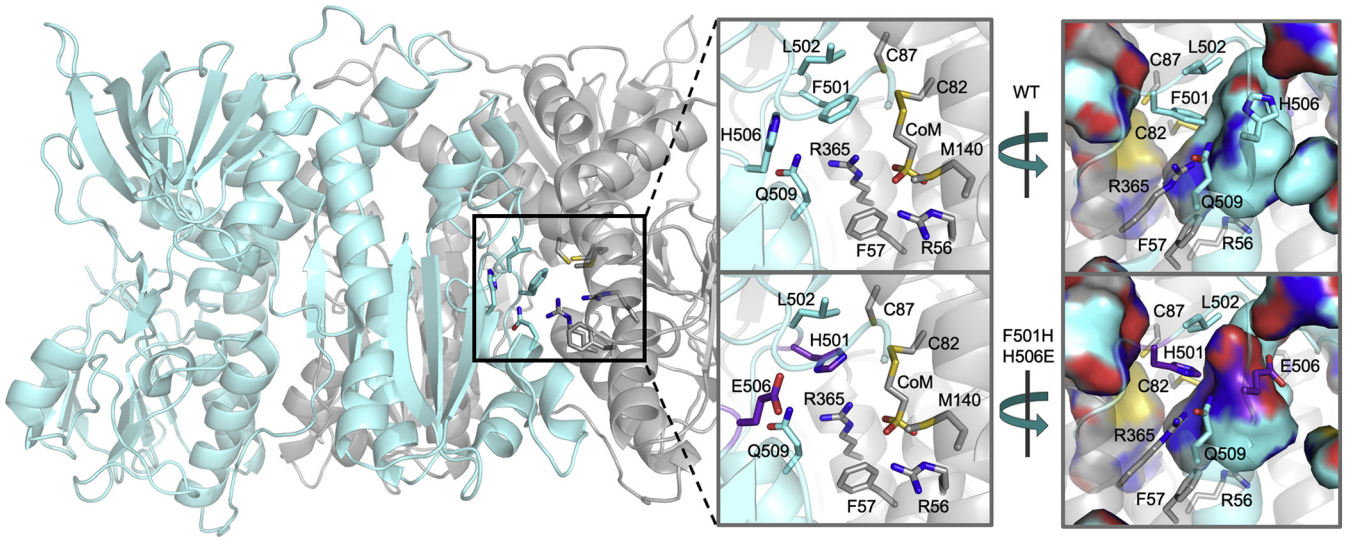


**Figure 4. Replacing the dyad to mimic DSORs changes the anionic pocket of 2-KPCC.** The structure of 2-KPCC is shown with one dimer colored *gray* and the other *cyan*. The active site, which resides at the dimer interface, is shown in the *black boxed area*. A close up of the anionic pocket in the WT active site is shown in the *top gray boxes*, whereas the F501H_H506E variant is shown in the *bottom two gray boxes*. The residues from one dimer are shown in *cyan* carbons, whereas the other dimers are shown in *gray* carbons. The substituted His at 501 and Glu at 506 are shown in *purple* carbons. Although the orientation of the DSOR-like His–Glu aligns with the WT Phe–His dyad, the active-site pocket size has decreased near the E506 residue. Protein Data Bank file of WT 2-KPCC: 2C3C; F501H_H506E variant: 7MGN. 2-KPCC, 2-ketopropyl coenzyme M oxidoreductase/carboxylase; DSORs, disulfide oxidoreductases.

KPCC H506E relative to F501H. Consistent with the slower rate of acetone production, NADPH turnover was ∼1.5-fold slower in H506E *versus* WT. Substrate turnover and product formation by the F501H_H506E double variant bore the hallmarks of each individual mutation. This variant exhibited no detectable acetoacetate production, instead making entirely acetone. Furthermore, the rate of acetone production was double that of the H506E single variant, consistent with the proposed active-site acid role for the H501.

As a second, more direct test of the role of H506 as an acetoacetate binding site, we examined acetoacetate as a possible product inhibitor. First, the initial rate of NADPH turnover ($v_i$) was measured as a function of variable 2-KPC concentration (1–5 mM) at a series of fixed concentrations (0–10 mM) of acetoacetate using WT 2-KPCC. The plots of $v_i$ *versus* [2-KPC] could each be fit to a rectangular hyperbolic function, consistent with the Michaelis–Menten model: $v_i = V_{max}[S]\,([S] + K_M)^{-1}$. The value of $V_{max}$ decreased as a function of increasing [acetoacetate], whereas the $K_M$ (2-KPC) remained approximately the same (Fig. 5).

If acetoacetate binds adjacent to H506, we reasoned that the H506E substitution should severely distort the electrostatic nature of the binding pocket, reduce or eliminate acetoacetate binding, and eliminate the inhibitory effects of acetoacetate. In fact, acetoacetate had no effect on catalysis by the H506E variant, even at concentrations up to 20 mM. These data further support a model where H506 is the site of enolacetone attack on $CO_2$ to form acetoacetate.

### *2-KPCC can use either its native or a DSOR-like reduced form to cleave the C–S bond of 2-KPC*

As described previously, F501 is an essential component of the 2-KPCC dyad, because it protects the enolacetone intermediate from reacting with a proton to make the toxic product, acetone. The DSOR-like F501H substitution contributes an acidic proton to the 2-KPCC active site, promoting this unwanted reaction.

The residue at position 501 serves a second crucial function in DSORs, including 2-KPCC, in maintaining the reduced enzyme in its reactive proton tautomer state (Fig. 1, *B* and *C*) (3). Specifically, the reduced and reactive form of DSORs is doubly protonated, at $Cys_{INT}$ and at the histidine from the catalytic dyad (Fig. 1*B*). The latter interacts electrostatically with $Cys_{CT}$, stabilizing the thiolate–FAD–CT interaction. By contrast, the hydrophobic F501 side chain in 2-KPCC stabilizes the $Cys_{CT}$ (C87) thiol ($Cys_{CT}$-SH), so that a CT is only observed at very high pH ($pK_a$ = 9.4 for the C82A variant) (3). At neutral pH, the reactive form of 2-KPCC has a single proton in its active site, which is shared between the $Cys_{INT}$ (C82) and $Cys_{CT}$ (C87) and fully transferred to the latter immediately prior to the reaction with 2-KPC (Fig. 1*C*) (3).

We hypothesized that 2-KPCC F501H could, like H487 in GR, stabilize a CT interaction with the FAD in the reduced state (Fig. 1*B*, *hashed line*). To test this, we measured the UV–visible spectra of the C82A_F501H double variant as a function of pH (Fig. 6). This variant lacks the $Cys_{INT}$ (C82); hence, all effects of pH on the active site will be confined either to the $Cys_{CT}$ (C87) or to H501. As with the C82A protein, a single pH transition from an FAD to an FAD-CT species was observed as the pH increased, though with a $pK_a$ shifted from 9.4 (C82A) to 8.2 (C82A_F501H). This indicates that the DSOR-like CT species is selectively stabilized by the F501H substitution.

We then asked whether the CT species in the F501H variant is capable of reacting with 2-KPC to form the mixed disulfide intermediate. To answer this question, we examined the reaction between reduced 2-KPCC and bromoethanesulfonate (BES), a 2-KPC surrogate that covalently modifies $Cys_{INT}$

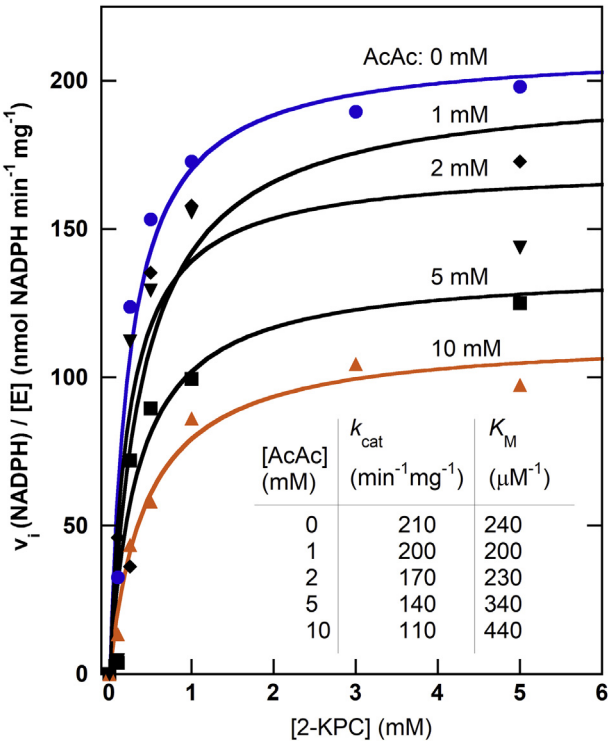


**Figure 5. Mixed noncompetitive inhibition of 2-KPC consumption is observed between WT 2-KPCC and acetoacetate.** Each curve was fit to the Michaelis–Menten equation, and apparent values for $k_{cat}$ and $K_M$ for each inhibitor concentration are tabulated. Changes in both parameters are consistent with a mixed noncompetitive inhibition pattern, where the acetoacetate product inhibitor binds both the free enzyme and enzyme–substrate complex at a site distinct from the location of substrate binding. We propose that this site is formed in part by the positive charge at H506. 2-KPC, 2-ketopropyl coenzyme M; 2-KPCC, 2-ketopropyl coenzyme M oxidoreductase/carboxylase.

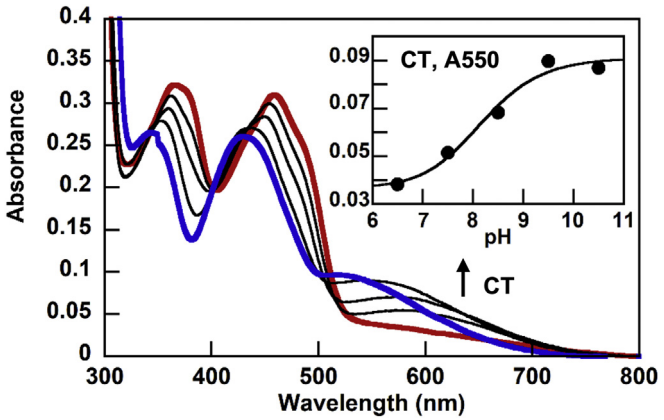


**Figure 6. The F501H substitution favors a DSOR-like active-site electronic structure.** The C82A_F501H double variant forms a $Cys_{CT}$ (C87)-flavin charge transfer (CT) adduct at alkaline pH with a p$K_a$ of 8.2, which is attributed to deprotonation of $Cys_{CT}$ (C87). The acidic spectrum (pH 6.5) is shown in *red*, and the alkaline spectrum (pH 10.5) is shown in *blue*. The alkaline form is a CT species in which the $Cys_{CT}$ (C87) interacts with the flavin. Intermediate pH spectra (pH 7.5, 8.5, and 9.5) are in *gray*. *Inset*, fitting the change in absorbance at 550 nm to the equation for a sigmoidal curve gives an apparent p$K_a$ of 8.2, which is significantly lower than the analogous transition for WT (p$K_a$ = 9.4). This suggests that H501, like the His in the canonical DSOR dyad, stabilizes the FAD/$Cys_{CT}$ (C87) CT interaction. DSOR, disulfide oxidoreductase; FAD, flavin adenine dinucleotide.

(C82) *via* alkylation when $Cys_{INT}$ (C82) is in its deprotonated form (Fig. 7) (21). Alkylation, which occurs when the active-site proton shifts from a shared position between $Cys_{INT}$ (C82) and $Cys_{CT}$ (C87), was detected *via* inactivation of the enzyme: that is, a fully modified enzyme exhibits no further reactivity toward NADPH, 2-KPC, and $CO_2$. In the plot of percent activity *versus* pH (Fig. 8), the inflection point is interpreted as the p$K_a$ for $Cys_{INT}$ (C82), since deprotonation of this residue leads synchronously to alkylation with BES. For WT 2-KPCC, this inflection point occurs near pH 8 (3), well below the p$K_a$ describing formation of the CT species and consistent with $Cys_{CT}$ (C87) acting as the base toward $Cys_{INT}$ (C82) (Fig. 1*C*). For the F501H substitution (single and double variants), the inflection point undergoes an alkaline shift of approximately 0.5 to 1 pH unit. Hence, the F501H substitution has a modest but measurable effect on the p$K_a$ for $Cys_{INT}$ (C82), slightly suppressing its reactivity. We speculate that, because the F501H substitution stabilizes the $Cys_{CT}$ (C87)-FAD CT interaction (p$K_a$ = 8.2; Fig. 6), the $Cys_{CT}$ (C87) is not available to act as a base toward the $Cys_{INT}$ (C82) proton. Rather, the H501 side chain of the F501H variant may instead act as the base toward $Cys_{INT}$ (C82), and the p$K_a$ near pH 9 in Figure 8 may be due to the deprotonation of H501, which catalyzes deprotonation of $Cys_{INT}$ (C82) in turn. Together, these data indicate that the F501H substitution stabilizes a DSOR-like protonation state in the reduced/reactive form of 2-KPCC, in which the $Cys_{CT}$ (C87) thiolate engages in a CT interaction with the FAD. In spite of being distinct from WT, this form of the protein is nonetheless reactive with 2-KPC. We propose that the histidine in F501H is capable of acting as a base toward $Cys_{INT}$ (C82), much like in a normal DSOR, removing the proton from the interchange thiol and catalyzing C–S bond cleavage within 2-KPC. This obviates the need for using $Cys_{CT}$ (C87) as an internal base.

## Conclusion

The carboxylation activity of 2-KPCC is unique among the DSOR family of enzymes. Although 2-KPCC exists with the conserved overall architecture and key elements important for Cys disulfide–dependent reductive bond cleavage, there are key elements that differ from other members of the family. We have proposed that these differences are important for carboxylation activity, most importantly the differences in the residues that constitute the catalytic dyad. The canonical DSOR catalytic dyad is key to stabilizing a specific thiol-reactive intermediate and providing protons for

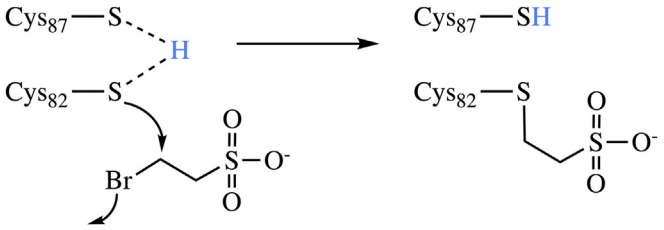


**Figure 7. Reaction of BES with $Cys_{INT}$ (C82) to form the alkylated complex.** BES, bromoethanesulfonate.

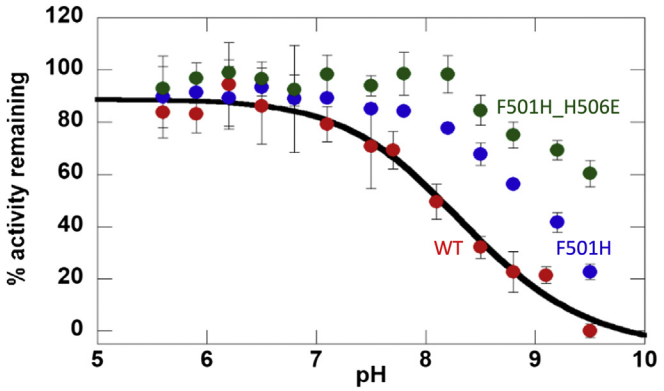


**Figure 8. The F501H variant reacts *via* the DSOR-like form of the active site.** Irreversible inactivation of 2-KPCC (WT and variants) by BES was monitored as a function of pH. Here, the measured p$K_a$ obtained by fitting a sigmoidal curve to the data is for the Cys that reacts with substrate ($Cys_{INT}$ (C82)), and the recipient base is $Cys_{CT}$ (C87). For the WT protein (*red circles*), this p$K_a$ is close to 8. For F501H (*blue circles*) and F501H_H506E (*green circles*), the p$K_a$ shifts closer to 9, again suggesting that protonation of $Cys_{CT}$ (C87) is destabilized in both variants. 2-KPCC, 2-ketopropyl-coenzyme M oxidoreductase/carboxylase; BES, bromoethanesulfonate; DSOR, disulfide oxidoreductase.

product formation. For 2-KPCC, coupling reductive cleavage with carboxylation adds an additional carboxylase-specific layer of criteria that needs to be satisfied, including the protection of the stabilized enolate intermediate from other attacking electrophiles like protons. Here, we provide compelling new insights through structural and biochemical analyses that the lack of conservation in the 2-KPCC catalytic dyad is of key mechanistic importance in allowing 2-KPCC to maintain its function in reductive cleavage and carboxylation activity. The substitution of Phe in 2-KPCC for the His observed in other members of the DSOR family promotes the formation of a different reactive intermediate and limits protons as competing electrophiles at the active site, suppressing the formation of the unproductive product acetone and promoting carboxylation. The substitution of His in 2-KPCC for Glu observed in other members of the DSOR family, in addition, helps form an anion binding pocket that stabilizes the developing charge incurred during acetoacetate formation.

## Experimental procedures

### *Expression and purification of native 2-KPCC and amino acid–substituted variants*

*Escherichia coli* BL21(DE3)pLysS or BL21(DE3) cells were transformed with the pBAD plasmid harboring the WT or corresponding variant 2-KPCC gene from *Xanthobacter autotrophicus* Py2. The construct contained a His affinity tag, a thioredoxin tag, and a tobacco etch virus cleavage site. Cells were plated on LB agar + kanamycin (25 μg/ml) plates and grown overnight. A single colony from the plate was used to inoculate a 5-ml overnight culture in LB + kanamycin (25 μg/ml). The 5 ml overnight culture was used as the inoculum for 500 ml of ZYP-rich media + kanamycin (25 μg/ml) in a baffled flask. Cells were grown at 37 °C with agitation at 225 rpm until the cultures reached an absorbance of 0.6 to 1.0. The temperature was reduced to 25 °C, L-arabinose was added to 0.02%, and the cells were grown for an additional 16 to 18 h. The cells were pelleted by centrifugation, frozen, and stored at −80 °C. The cell pellet was resuspended in four volumes of lysis buffer (20 mM Tris, pH 8.0, 300 mM NaCl, 5 mM imidazole, and protease inhibitor tablet [Pierce]) and thawed at 30 °C. All subsequent treatments were performed on ice or at 4 °C. The resuspended cells were lysed *via* multiple rounds of sonication (Branson Ultrasonifier). Cell lysates were clarified *via* centrifugation at 75,000*g* for 45 min. Clarified lysates were loaded onto a nickel–nitrilotriacetic acid resin column (Bio-Rad) *via* a Bio-Rad FPLC, washed with lysis buffer, and eluted using a 0.005 to 0.4 M imidazole gradient in lysis buffer at 3 ml/min. The eluted 2-KPCC was diluted sixfold into buffer A (20 mM Tris, pH 6.5, and 5% w/v glycerol), applied to a DEAE-Sepharose ion-exchange column (Bio-Rad), and eluted using a 0 to 1 M NaCl gradient in buffer A. Fractions were screened using SDS-PAGE. Pure 2-KPCC protein was pooled and run on a desalting column (Bio-Rad) in 20 mM Tris, pH 7.4, 10% glycerol, and 200 mM NaCl. Protein was concentrated using a 30 K molecular weight cutoff spin filter concentrator. Total protein concentration was determined using a bicinchoninic protein assay (Thermo Scientific), whereas flavin concentration was determined from its UV–visible absorbance at 450 nm using an ε450 of 11,828 $M^{-1}$ $cm^{-1}$. All concentrations of protein cited in the text refer to flavin-containing protein.

### *Crystal growth and structure determination*

The crystals for this study were obtained by the vapor diffusion method. The purified F501H and F501H_H506E 2-KPCC (20 mg/ml) were incubated with substrate 2-KPC or CoM (10 mM final concentration), respectively, for 10 min prior to addition of an equal amount of precipitating solution containing 0.17 M ammonium acetate, 0.085 M trisodium citrate, pH 5.6, 27% PEG 4000, and 15% glycerol. Crystals in the form of clusters of lathes appeared after 1 week of incubation. They belong to the monoclinic space group with one dimer per asymmetric unit and cell dimensions a = 87.05 Å, b = 60.21 Å, c = 104.86 Å, and α = γ = 90°, and β = 100.46°. Data were collected from single plate flash-cooled crystals with a continuous flow of liquid nitrogen at 100 K at Stanford Synchrotron Radiation Lightsource beamline 12-2 equipped with a PILATUS detector with 0.15° oscillation.

The diffraction images were indexed, integrated, and scaled using HKL2000 (22) or XDS (23). The F501H and F501H_H506E 2-KPCC structures were solved by the molecular replacement method using the mixed-disulfide crystal structure of 2-KPCC (Protein Data Bank [PDB] code: 2C3C) as a search model with Phaser of the CCP4 program suite (24).

The solutions were refined and improved by phenix.refine. Model building was subsequently completed manually using Coot software (The University of Oxford) (25). Figures were prepared using PyMol (Schrodinger) (26). F501H and F501H_H506E 2-KPCC structures were deposited in the PDB with code 7MGO and 7MGN, respectively. The data

processing and refinement statistics for these structures are given in Table S1.

### Monitoring UV–visible changes in the flavin species in 2-KPCC variant as a function of pH

All pH titrations were carried out anerobically in a Coy anerobic chamber. Samples contained 20 μM 2-KPCC, 100 μM $NADP^+$, 100 mM glycine/Tris/phosphate buffer and were conducted using a procedure similar to that described by Kofoed *et al.* (27). Samples were loaded into gas tight cuvettes, and the reaction was monitored using an Agilent Cary UV–visible NIR spectrophotometer.

### BES inactivation

All reactions were conducted under nitrogen (~2% $H_2$) in an anerobic chamber (Coy Lab Products). Solutions of 100 mM buffers were made at varying pH from Tris base, $K_3PO_4$, and glycine. DTT and BES from the concentrated stocks were added to each solution to give final concentrations of 5 mM BES and 10 mM DTT. A control sample that lacked BES was run in parallel. The samples were allowed to incubate at 20 °C for 4 h. This incubation time was previously shown (3) to result in a range of enzyme reactivity with BES, from <10% to nearly stoichiometric, depending on the pH. It was concluded that increasing pH therefore shifts the proton tautomerization state, from a position where it is shared between $Cys_{INT}/Cys_{CT}$ and $Cys_{CT}$. To remove unreacted BES, samples were treated with DOWEX resin as previously described (27). Each sample was assayed for residual activity *via* addition of the BES-treated enzyme to a 5 mM 2-KPC and 0.1 mM NADPH solution made in 100 mM GTP buffer at pH 7. The initial rates of NADPH consumption were monitored at 340 nm using an Agilent 8453 spectrometer equipped with a diode array detector and compared with the sample control. Triplicate technical replicates were carried out for WT, F501H, and F501H_H506E 2-KPCC.

### Kinetic/functional assays and product analyses

Acetoacetate production was measured using the coupled β-hydroxybutyrate dehydrogenase (β-HBDH) assay as previously described (2, 21) using a BMG Labtech CLARIOstar microplate reader in reaction volumes of 200 μl. Under excess β-HBDH, acetoacetate produced by 2-KPCC is coupled to NADH oxidation by the reverse reaction of β-HBDH. The reaction mixture contained 0.25 mg 2-KPCC, 10 mM DTT (as the reducing agent instead of NADPH), 60 mM $KHCO_3$, 0.2 mM NADH, and the reaction was initiated by injecting 5 mM 2-KPC. Reactions were conducted in a 100 mM Tris at pH 7.4 buffer. Rates of NADH oxidization, observed by the decrease in the absorbance at 340 nm, are proportional to acetoacetate production.

The rate of NADPH oxidation was measured as the time-dependent decrease in the absorbance at 340 nm on an Agilent Cary UV–visible NIR spectrophotometer in reaction volumes of 500 μl. The reaction contained 0.2 mM NADPH, 0.25 mg 2-KPCC, 60 mM $KHCO_3$, and the reaction was initiated by adding 5 mM 2-KPC. Reactions were conducted in a 100 mM Tris at pH 7.4 buffer. Assays were analyzed in triplicate.

The off-pathway product acetone was quantified *via* 100 μl headspace injections on a ThermoFisher GC Trace 1300 using buffer degassed on a vacuum/nitrogen gas manifold in series with a $CO_2$ scrub KOH trap. The standard assay contained 100 mM Tris at pH 7.4, 10 mM DTT, 0.25 mg 2-KPCC, and 5 mM 2-KPC in a 10 ml crimp-sealed vial. After 50 min incubation at 30 °C and 180 rpm, $KHCO_3$ (60 mM) was added *via* syringe as a source of $CO_2$ substrate. The difference in rates of activities measured by the GC and the UV–visible coupled assay from the NADPH oxidation assay (Table 1) can be attributed to the use of the non-natural reductant DTT as opposed to the physiological reductant NADPH.

Acetoacetate inhibition assays were performed at varying concentrations of acetoacetate (0–10 mM), monitoring 2-KPC–dependent oxidation of NADPH at 340 nm. The standard assay mixture contained 100 mM Tris at pH 7.4, 0.5 mM NADPH, 60 mM $KHCO_3$, and 0.25 mg 2-KPCC. Assays were initiated by addition of substrate 2-KPC and monitored with a BMG Labtech CLARIOstar plate reader in reaction volumes of 200 μl.

Kinetic constants ($K_M$ and $V_{max}$) were calculated by fitting initial rate data to the Michaelis–Menten equation using Kaleidagraph software (Kaleidagraph).

## Data availability

X-ray crystal structure data that support the findings of this study have been deposited in the Worldwide PDB. The PDB accession codes for the F501H and double F501H_H506E 2-KPCC variants are 7MGO and 7MGN, respectively. All other data are contained within this article and supporting information.

*Supporting information*—This article contains supporting information.

*Acknowledgments*—Use of the Stanford Synchrotron Radiation Lightsource, SLAC National Accelerator Laboratory, is supported by the US Department of Energy (DOE), Office of Science, Basic Energy Sciences, under contract number DE-AC02-76SF00515. The Stanford Synchotron Radiation Lightsource Structural Molecular Biology Program is supported by the DOE Office of Biological and Environmental Research and the National Institutes of Health, National Institute of General Medical Sciences (including grant no. P41GM103393). Computer resources were provided by the W. R. Wiley Environmental Molecular Sciences Laboratory, a DOE Office of Science User Facility located at Pacific Northwest National Laboratory and sponsored by the Office of Biological and Environmental Research of DOE.

*Author contributions*—J. L. D. and J. W. P. methodology; G. A. P. and K. A. S. investigation; G. A. P., K. A. S., O. A. Z., and B. R. S. data curation; K. A. S. and J. L. D. writing-original draft; G. A. P., K. A. S., O. A. Z., B. R. S., J. L. D., and J. W. P. writing-review and editing; J. W. P. supervision; J. W. P. project administration; J. W. P. funding acquisition.

*Funding and additional information*—This work was supported by the US DOE, Office of Science, Office of Basic Energy Sciences under award DE-SC0018143 to J. W. P. and J. L. D. Partial salary support for J. W. P. was supported by the United States Department of Agriculture National Institute of Food and Agriculture, Hatch umbrella project #1015621. The content is solely the responsibility of the authors and does not necessarily represent the official views of the funding agencies.

*Conflict of interest*—The authors declare that they have no conflict of interest with the contents of this article.

*Abbreviations*—The abbreviations used are: 2-KPC, 2-ketopropyl-coenzyme M; 2-KPCC, 2-ketopropyl-coenzyme M oxidoreductase/carboxylase; β-HBDH, β-hydroxybutyrate dehydrogenase; BES, bromoethanesulfonate; CT, charge transfer; DOE, Department of Energy; DSOR, disulfide oxidoreductase; FAD, flavin adenine dinucleotide; GR, glutathione reductase; PDB, Protein Data Bank.

## References

1. Glueck, S. M., Gumus, S., Fabian, W. M., and Faber, K. (2010) Biocatalytic carboxylation. *Chem. Soc. Rev.* **39**, 313–328
2. Prussia, G. A., Gauss, G. H., Mus, F., Conner, L., DuBois, J. L., and Peters, J. W. (2016) Substitution of a conserved catalytic dyad into 2-KPCC causes loss of carboxylation activity. *FEBS Lett.* **590**, 2991–2996
3. Streit, B. R., Mattice, J. R., Prussia, G. A., Peters, J. W., and DuBois, J. L. (2019) The reactive form of a C-S bond-cleaving, CO2-fixing flavoenzyme. *J. Biol. Chem.* **294**, 5137–5145
4. Ghisla, S., and Massey, V. (1989) Mechanisms of flavoprotein-catalyzed reactions. *Eur. J. Biochem.* **181**, 1–17
5. Pai, E. F. (1991) Variations on a theme: The family of FAD-dependent NAD(P)H-(disulfide)-oxidoreductases. *Curr. Opin. Struct. Biol.* **1**, 796–803
6. Williams, C. H. J. (1992) Lipoamide dehydrogenase, glutathione reductase, thioredoxin reductase, and mercuric ion reductase – a family of flavoenzyme transhydrogenases. In Muller, F., ed., *Chemistry and Biochemistry of Flavoenzymes* (Vol 3,. CRC Press, Boca Raton, FL: 121–211
7. Deponte, M. (2013) Glutathione catalysis and the reaction mechanisms of glutathione-dependent enzymes. *Biochim. Biophys. Acta* **1830**, 3217–3266
8. Karplus, P. A., and Schulz, G. E. (1989) Substrate binding and catalysis by glutathione reductase as derived from refined enzyme: Substrate crystal structures at 2 A resolution. *J. Mol. Biol.* **210**, 163–180
9. Pai, E. F., and Schulz, G. E. (1983) The catalytic mechanism of glutathione reductase as derived from x-ray diffraction analyses of reaction intermediates. *J. Biol. Chem.* **258**, 1752–1757
10. Schulz, G. E., Schirmer, R. H., Sachsenheimer, W., and Pai, E. F. (1978) The structure of the flavoenzyme glutathione reductase. *Nature* **273**, 120–124
11. Rietveld, P., Arscott, L. D., Berry, A., Scrutton, N. S., Deonarain, M. P., Perham, R. N., and Williams, C. H., Jr. (1994) Reductive and oxidative half-reactions of glutathione reductase from Escherichia coli. *Biochemistry* **33**, 13888–13895
12. Deonarain, M. P., Berry, A., Scrutton, N. S., and Perham, R. N. (1989) Alternative proton donors/acceptors in the catalytic mechanism of the glutathione reductase of Escherichia coli: The role of histidine-439 and tyrosine-99. *Biochemistry* **28**, 9602–9607
13. Clark, D. D., Allen, J. R., and Ensign, S. A. (2000) Characterization of five catalytic activities associated with the NADPH:2-ketopropyl-coenzyme M [2-(2-ketopropylthio)ethanesulfonate] oxidoreductase/carboxylase of the Xanthobacter strain Py2 epoxide carboxylase system. *Biochemistry* **39**, 1294–1304
14. Nocek, B., Jang, S. B., Jeong, M. S., Clark, D. D., Ensign, S. A., and Peters, J. W. (2002) Structural basis for CO2 fixation by a novel member of the disulfide oxidoreductase family of enzymes, 2-ketopropyl-coenzyme M oxidoreductase/carboxylase. *Biochemistry* **41**, 12907–12913
15. Pandey, A. S., Nocek, B., Clark, D. D., Ensign, S. A., and Peters, J. W. (2006) Mechanistic implications of the structure of the mixed-disulfide intermediate of the disulfide oxidoreductase, 2-ketopropyl-coenzyme M oxidoreductase/carboxylase. *Biochemistry* **45**, 113–120
16. Argyrou, A., and Blanchard, J. S. (2004) Flavoprotein disulfide reductases: Advances in chemistry and function. *Prog. Nucleic Acid Res. Mol. Biol.* **78**, 89–142
17. Ensign, S. A., and Allen, J. R. (2003) Aliphatic epoxide carboxylation. *Annu. Rev. Biochem.* **72**, 55–76
18. Frey, P. A., and Hegeman, A. D. (2007) Decarboxylation and carboxylation. In *Enzymatic Reaction Mechanism*, Oxford University Press, New York, NY: 387–426
19. Cleland, W. W., Andrews, T. J., Gutteridge, S., Hartman, F. C., and Lorimer, G. H. (1998) Mechanism of Rubisco: The carbamate as general base. *Chem. Rev.* **98**, 549–562
20. Pandey, A. S., Mulder, D. W., Ensign, S. A., and Peters, J. W. (2011) Structural basis for carbon dioxide binding by 2-ketopropyl coenzyme M oxidoreductase/carboxylase. *FEBS Lett.* **585**, 459–464
21. Boyd, J. M., Clark, D. D., Kofoed, M. A., and Ensign, S. A. (2010) Mechanism of inhibition of aliphatic epoxide carboxylation by the coenzyme M analog 2-bromoethanesulfonate. *J. Biol. Chem.* **285**, 25232–25242
22. Otwinowski, Z., and Minor, W. (1997) Processing of X-ray diffraction data collected in oscillation mode. *Methods Enzymol.* **276**, 307–326
23. Kabsch, W. (2010) XDS. *Acta Crystallogr. D Biol. Crystallogr.* **66**, 125–132
24. McCoy, A. J., Grosse-Kunstleve, R. W., Adams, P. D., Winn, M. D., Storoni, L. C., and Read, R. J. (2007) Phaser crystallographic software. *J. Appl. Crystallogr.* **40**, 658–674
25. Emsley, P., and Cowtan, K. (2004) Coot: Model-building tools for molecular graphics. *Acta Crystallogr. D Biol. Crystallogr.* **60**, 2126–2132
26. Delano, W. L. (2002) *The PyMOL Molecular Graphics System*, Delano Scientific, San Carlos, CA
27. Kofoed, M. A., Wampler, D. A., Pandey, A. S., Peters, J. W., and Ensign, S. A. (2011) Roles of the redox-active disulfide and histidine residues forming a catalytic dyad in reactions catalyzed by 2-ketopropyl coenzyme M oxidoreductase/carboxylase. *J. Bacteriol.* **193**, 4904–4913